

Are James Webb Space Telescope observations consistent with warm dark matter?

Bruce Hoeneisen

Universidad San Francisco de Quito, Quito, Ecuador

Email: bhoeneisen@usfq.edu.ec

16 January 2024

Abstract

We compare observed with predicted distributions of galaxy stellar masses M_* and galaxy rest-frame ultra-violet luminosities per unit bandwidth L_{UV} , in the redshift range $z = 2$ to 13. The comparison is presented as a function of the comoving warm dark matter free-streaming cut-off wavenumber k_{fs} . For this comparison the theory is a minimal extension of the Press-Schechter formalism with only two parameters: the star formation efficiency, and a proportionality factor between the star formation rate per galaxy and L_{UV} . These two parameters are fixed to their values obtained prior to the James Webb Space Telescope (JWST) data. The purpose of this comparison is to identify if, and where, detailed astrophysical evolution is needed to account for the new JWST observations.

Keywords

James Webb Space Telescope, JWST, Warm Dark Matter.

1 Introduction

Early James Webb Space Telescope (JWST) observations were surprising: they reveal galaxies at high redshifts ($z \gtrsim 10$) with greater number densities than predicted by the “ Λ CDM cosmology”. A list of surprises from the first observations of JWST, and of several proposed modifications of the theory to account for this data, is summarized in [1]. The “ Λ CDM cosmology” that is actually compared with the new JWST data is an extension of the 6-parameter Λ CDM cosmology with a dozen, or so, astrophysical parameters [2].

The purpose of the present study is two-fold: a) To extend the comparison between observations and predictions to include warm dark matter, and b) to make the comparison with a “first-order” prediction, that has as few, physically motivated, adjustable parameters as possible, with these parameters determined numerically from observations prior to JWST data, leaving zero new degrees of freedom for the comparison. The idea is to clearly identify regions of parameter space that require a more detailed cosmological and/or astrophysical description to understand the evolution of the observations.

We focus our attention on distributions of the galaxy stellar masses M_* and of the galaxy rest-frame ultra-violet (UV) luminosities per unit bandwidth L_{UV} , that can be predicted with the Press-Schechter formalism given three parameters: the warm dark matter power spectrum cut-off wavenumber k_{fs} , the stellar formation efficiency f_* , and a proportionality factor between the star formation rate per galaxy (SFR) and L_{UV} .

The outline of the article is as follows. In Section 2 we compare observed and predicted distributions of M_* and L_{UV} for redshifts z in the range 2 to 13. The “first order” theory turns out to be in agreement with most of the data. There are, however, three parameter regions with tensions. In Section 3 we describe the data. In Section 4 we present the details of how we include warm dark matter in the Press-Schechter formalism. With these preparations we are able to discuss the observed tensions in Section 5. We close with conclusions.

2 Comparison of observed distributions of M_* and L_{UV} with predictions

In Figure 1 we compare observed distributions of galaxy stellar masses M_* (top panel) and galaxy rest-frame ultra-violet luminosities per unit bandwidth L_{UV} (bottom panel) with “first-order” predictions at redshift $z = 6$. The data is obtained from Hubble Space Telescope (HST) observations (black squares) [3] [4], from the continuity equation [5] (red triangles), and from the James Webb Space Telescope (JWST) observations (green triangles) [6]. A description of this data is postponed to Section 3.

Experimenters obtain the galaxy absolute magnitude $M_{1600,AB}$ in the AB system [7] at the rest frame wavelength $\approx 1600 \text{ \AA}$ in the ultra-violet (UV). This absolute magnitude is related to the galaxy radiated power per unit bandwidth L_{1600} as follows:

$$M_{1600,AB} = +51.6 - 2.5 \log_{10} L_{UV}, \quad (1)$$

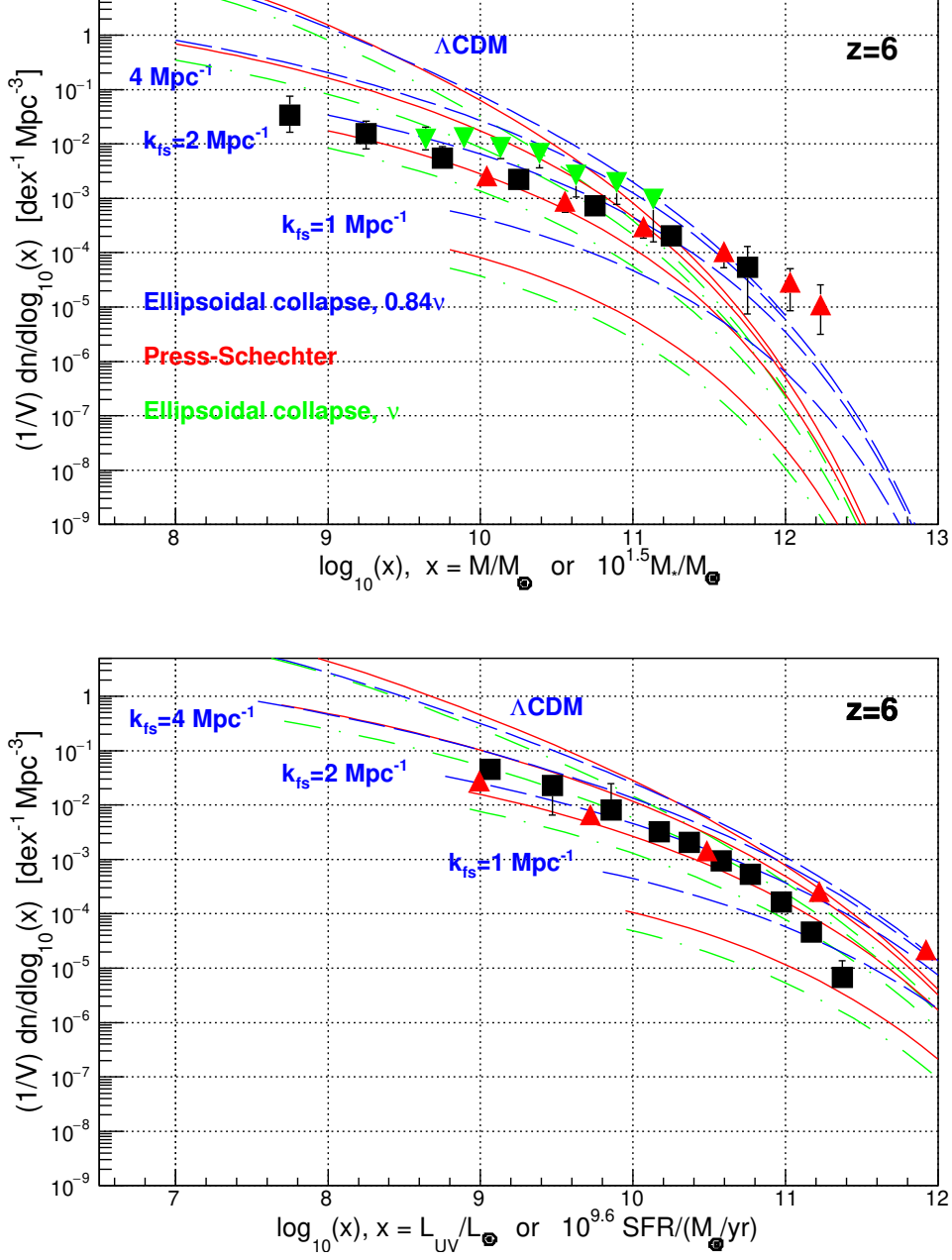


Figure 1: Comparison of predicted and observed distributions of $M/M_{\odot} = 10^{1.5} M_*/M_{\odot}$ (top panel) and $L_{UV}/L_{\odot} = 10^{9.6} \text{SFR}/(M_{\odot}/\text{yr})$ (bottom panel) for redshift $z = 6$. Data are from the Hubble Space Telescope (M_* from [3] and L_{UV} from [4]) (black squares), from the continuity equation [5] (red triangles), and from the James Webb Space Telescope (green triangles) [6].

where $L_{UV} \equiv L_{1600}/(\text{erg s}^{-1} \text{ Hz}^{-1})$ (from the definition of absolute M_{AB} in [7]). In comparison, the absolute magnitude of the Sun at wavelength 3900 Å is [8]

$$M_{3900,\odot,AB} = 5.9 = +51.6 - 2.5 \log_{10} L_{\odot}, \quad (2)$$

where $L_{\odot} \equiv L_{3900,\odot}/(\text{erg s}^{-1} \text{ Hz}^{-1})$. Note that the solar flux power per unit wavelength is a maximum near 3900 Å. We plot distributions of M_*/M_{\odot} and L_{UV}/L_{\odot} . L_{UV}/L_{\odot} is obtained from $M_{1600,AB}$ as follows:

$$M_{1600,AB} \equiv 5.9 - 2.5 \log_{10} \left(\frac{L_{UV}}{L_{\odot}} \right). \quad (3)$$

This definition of L_{UV}/L_{\odot} , that is somewhat arbitrary, is chosen because it gives a physical sense of luminosity in solar units, and also because $M/M_{\odot} \approx L_{UV}/L_{\odot}$ at $z = 6$, see Figure 1.

The predictions are an extension of the Press-Schechter formalism to include warm dark matter (as described in Section 4). The “warmness” of the dark matter is defined by the comoving power spectrum cut-off wavenumber k_{fs} due to dark matter free-streaming in and out of density minimums and maximums. We present predictions corresponding to $k_{fs} = 1, 2, 4$ and 200 Mpc^{-1} . The latter large value of k_{fs} , corresponding to negligible free-streaming, is identified with the cold dark matter Λ CDM cosmology. We present Press-Schechter predictions [9], and two Sheth-Mo-Tormen ellipsoidal collapse extensions [10] [11]. Presenting three predictions for each k_{fs} illustrates the uncertainties of these predictions. The predictions obtain the distributions of the *linear* perturbation total (dark matter plus baryon) masses M as defined by the Press-Schechter formalism (see Section 4). The predicted number of galaxies per unit volume and per decade of M , $(1/V) \cdot dn/d \log_{10}(M/M_{\odot})$, with units $[\text{dex}^{-1} \text{ Mpc}^{-3}]$, is a function of M , z and k_{fs} . Therefore it is still necessary to find relations between M_* and L_{UV} with M . We consider the simplest relations, i.e. M_* proportional to M , and L_{UV} proportional to the star formation rate per galaxy (SFR), with units $[M_{\odot}/\text{yr}]$. The proportionality of L_{UV} with SFR is justified because L_{UV} is dominated by large mass stars with lifetimes τ short compared to the age of the universe $t(z)$ at redshift z [12]. Then

$$M_* \equiv 10^{-a} M \equiv f_* \frac{\Omega_b}{\Omega_c + \Omega_b} M, \quad (4)$$

$$\frac{L_{UV}}{L_{\odot}} \equiv 10^b \frac{\text{SFR}}{M_{\odot}/\text{yr}}, \quad (5)$$

which define the parameters a , f_* and b . Ω_b and Ω_c are the mean densities of baryons and dark matter in units of the critical density (throughout we

use the notation and parameter values of [7]). f_* is defined to be the “star formation efficiency”. Given (M, z, k_{fs}) we predict

$$\text{SFR} \equiv 10^{-a} \frac{M \, dn/d \log_{10}(M/M_{\odot}) - dn'/d \log_{10}(M/M_{\odot})}{\tau \, dn/d \log_{10}(M/M_{\odot})}, \quad (6)$$

where $dn/d \log_{10}(M/M_{\odot})$ is calculated at (M, z, k_{fs}) , and $dn'/d \log_{10}(M/M_{\odot})$ is calculated at (M, z', k_{fs}) , where the age of the universe at redshift z is $t(z)$, and the age of the universe at redshift z' is $t(z') = t(z) - \tau$, in the limit of small τ , i.e. $\tau \ll t(z)$.

In summary, the predictions for each k_{fs} depend on only the two parameters a and b . These parameters are in principle functions of M , z and k_{fs} . However, for the purpose of comparisons with the data, we assume that a and b are constants. Note that varying a and b shifts the predictions in Figure 1 to the right or to the left. For the comparisons we choose values of a and b obtained *prior* to JWST data [13] [14]:

$$a = 1.5 \quad \text{and} \quad b = 9.6. \quad (7)$$

These values of a and b define our “first-order” predictions. $a = 1.5$ corresponds to a star formation efficiency $f_* = 0.20$ (taken to be independent of z in our “first-order” predictions!). For a Salpeter initial mass function (IMF), and L_{UV} measured at a rest frame wavelength $\approx 1500\text{\AA}$, the following L_{UV} is obtained in [12]:

$$L_{UV} = 8 \times 10^{27} \frac{\text{SFR}}{M_{\odot}/\text{yr}}. \quad (8)$$

Then, from (2), (5) and (8), we obtain $b = 9.6$. The value of k_{fs} measured *prior* to JWST data is [14]

$$k_{fs} = 2.0_{-0.5}^{+0.8} \text{ Mpc}^{-1}. \quad (9)$$

Comparisons of observed distributions of M_*/M_{\odot} and L_{UV}/L_{\odot} with first-order predictions, for redshift z in the range 2 to 13, are presented in Figures 1 to 5. Sometimes we omit the “Press-Schechter” and “Ellipsoidal Collapse, ν ” predictions for clarity. For future reference we also present predictions for $z = 15$ in Figure 5. The predictions are presented for $M \gtrsim M_{vd}$, where M_{vd} is the velocity dispersion limit of validity of the predictions [14]: for $M \lesssim M_{vd}$ the density fluctuation does not collapse gravitationally. We find agreement of the measurements with the first-order predictions in most of the parameter space, so these predictions are a good starting point to develop a more detailed theory.

There are however three discrepant regions:

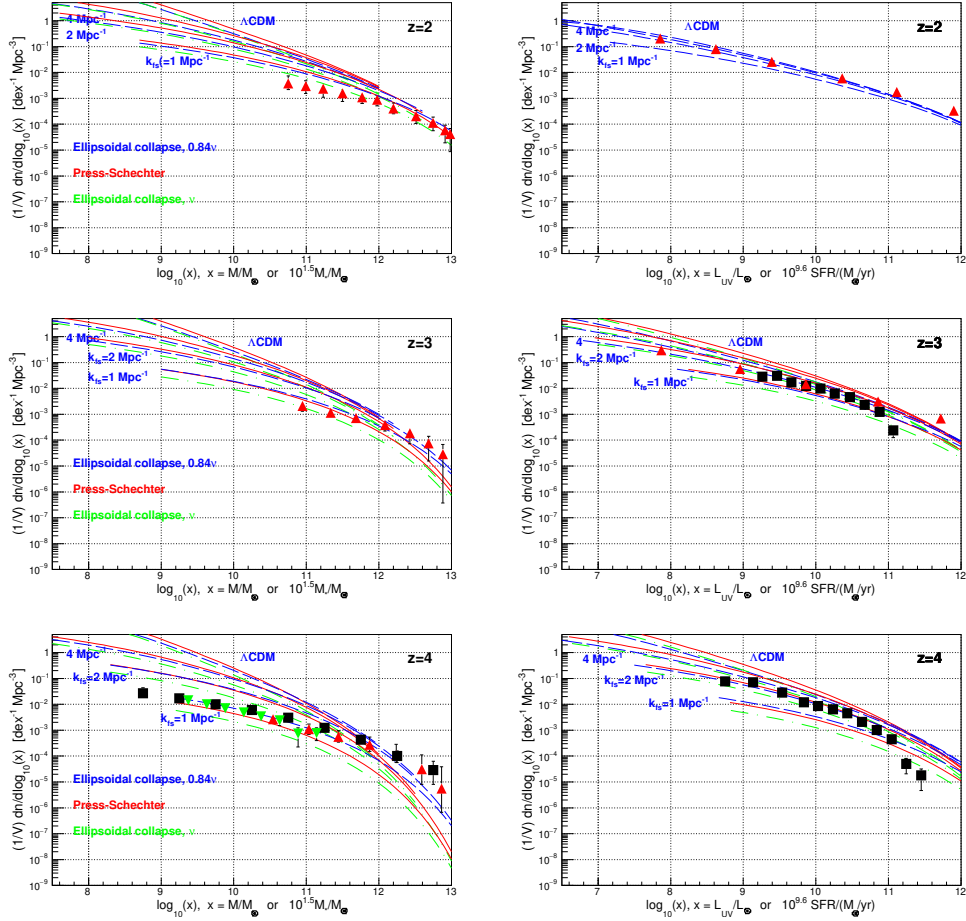


Figure 2: Comparison of predicted and observed distributions of $M/M_{\odot} = 10^{1.5} M_{*}/M_{\odot}$ (left panels) and $L_{UV}/L_{\odot} = 10^{9.6} \text{SFR}/(M_{\odot}/\text{yr})$ (right panels) for redshift $z = 2$ (top row), 3 and 4 (bottom row). Data are from the Hubble Space Telescope (black squares) (M_{*} from [3] and L_{UV} from [4]), from the continuity equation [5] (red triangles), and from the James Webb Space Telescope (green triangles) [6].

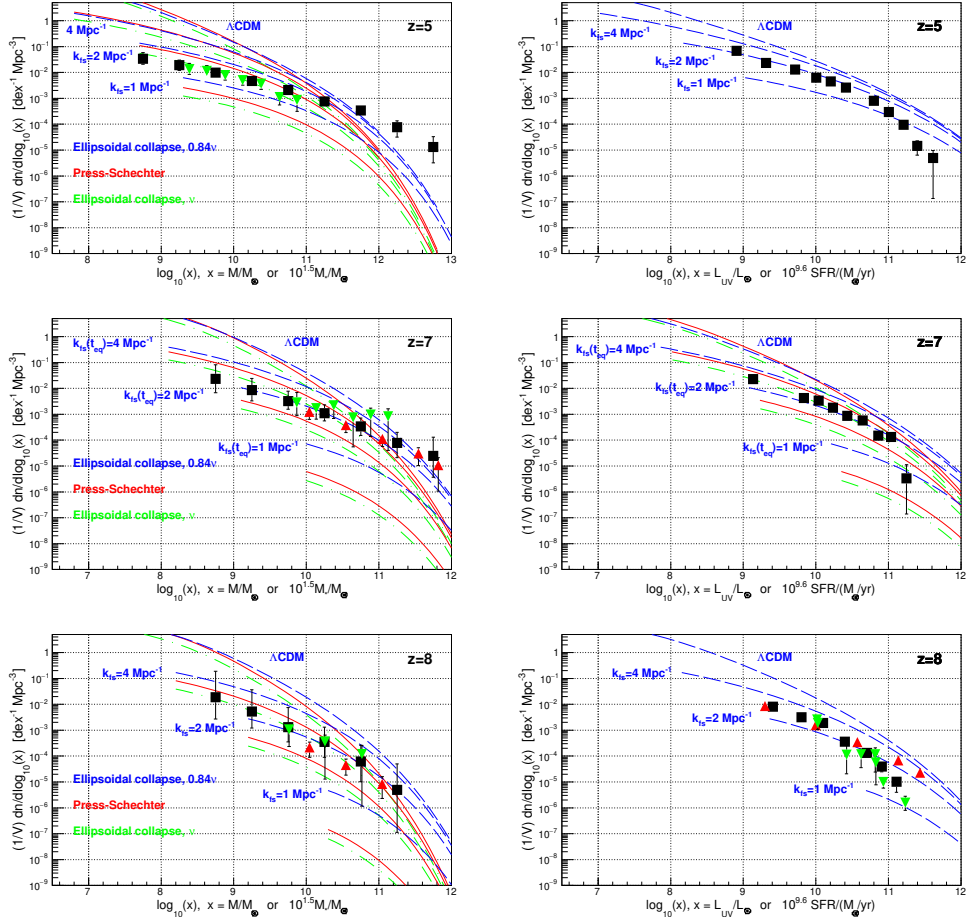


Figure 3: Comparison of predicted and observed distributions of $M/M_\odot = 10^{1.5} M_*/M_\odot$ (left panels) and $L_{UV}/L_\odot = 10^{9.6} \text{SFR}/(M_\odot/\text{yr})$ (right panels) for redshift $z = 5$ (top row), 7 and 8 (bottom row). Data are from the Hubble Space Telescope (black squares) (M_* from [3] and L_{UV} from [4]), from the continuity equation [5] (red triangles), and from the James Webb Space Telescope (green triangles) (M_* from [6] and L_{UV} from [15], [16], [17]).

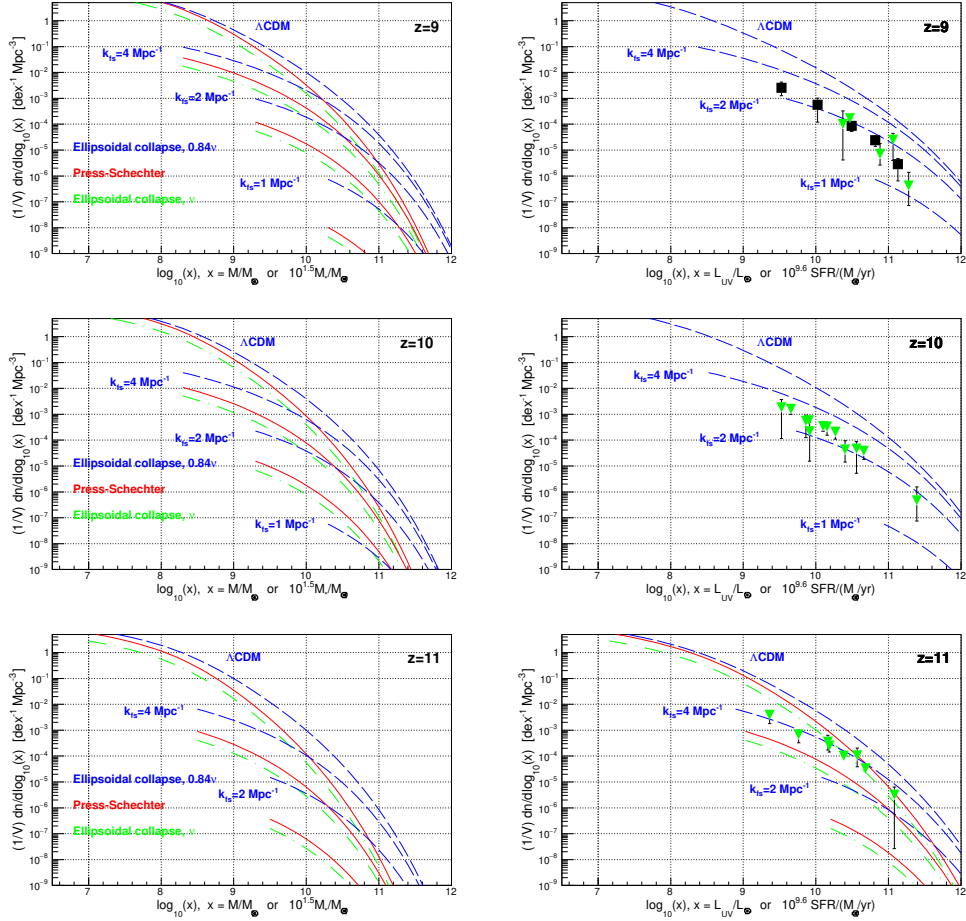


Figure 4: Comparison of predicted and observed distributions of $M/M_{\odot} = 10^{1.5} M_{*}/M_{\odot}$ (left panels with no data) and $L_{UV}/L_{\odot} = 10^{9.6} \text{SFR}/(M_{\odot}/\text{yr})$ (right panels) for redshift $z = 9$ (top row), 10 and 11 (bottom row). Data are from the Hubble Space Telescope (black squares) (L_{UV} from [4]), and from the James Webb Space Telescope (green triangles) (L_{UV} from [15], [16], [17], [18], [19], [20], [21]).

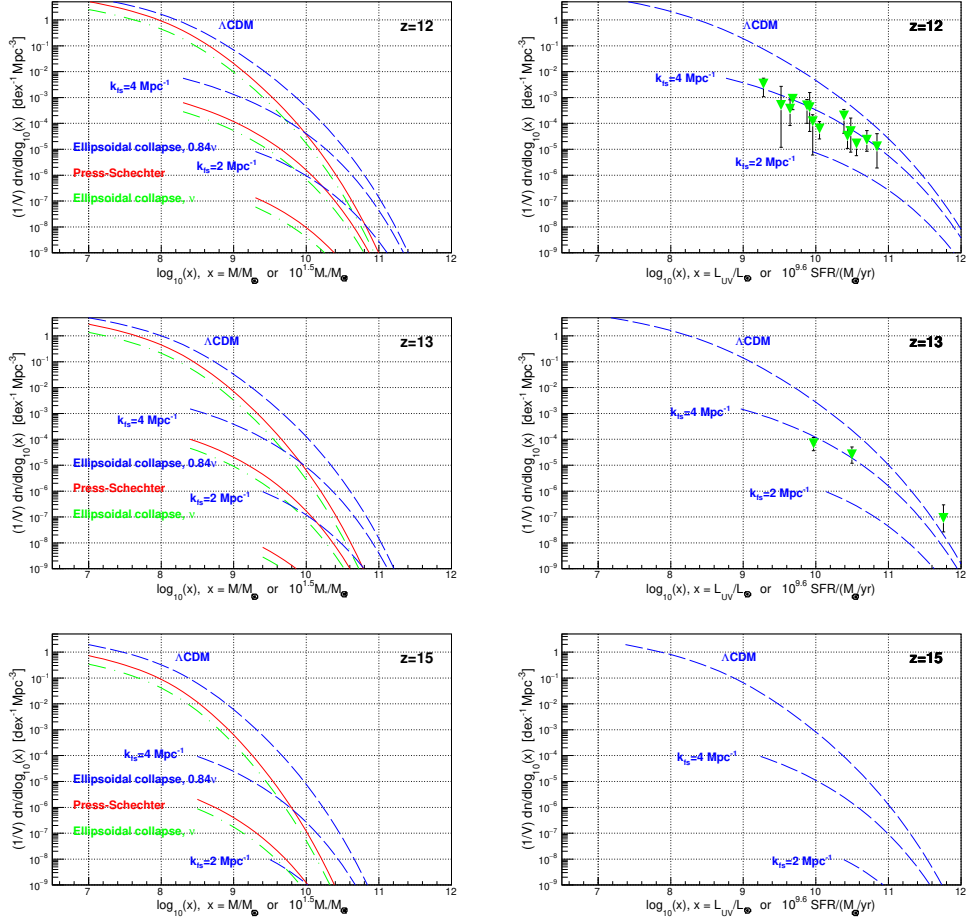


Figure 5: Comparison of predicted and observed distributions of $M/M_\odot = 10^{1.5} M_*/M_\odot$ (left panels with no data) and $L_{UV}/L_\odot = 10^{9.6} \text{SFR}/(M_\odot/\text{yr})$ (right panels) for redshift $z = 12$ (top row), 13 and 15 (bottom row). Data are from the James Webb Space Telescope (green triangles) (L_{UV} from [15], [16], [17], [18], [19], [21], [22], [23]).

1. Discrepancies of L_{UV} distributions at $L_{UV}/L_{\odot} \gtrsim 10^{10.7}$ and $3 \lesssim z \lesssim 9$.
2. Discrepancies of M_* distributions at $z \lesssim 5$.
3. Discrepancies with preliminary JWST observations of L_{UV} distributions at $z \gtrsim 11$.

The first and second discrepancies are common to cold and warm dark matter.

We will discuss these discrepancies in Section 5. However, before doing so, we need to understand the data sources, and the warm dark matter extension of the theory.

3 Data

For $z = 2$ to 10 we obtain the distributions of magnitude $M_{1600,AB}$ from Table 4 of [4] (for $z = 10$ the results are from [24]). These measurements have black square markers in Figures 1 to 4. The data in these references are obtained from Hubble Space Telescope (HST) observations in approximately 11 filter bands (to obtain the photometric z with stellar population synthesis (SPS) models), i.e. $UV_{275}, B_{435}, V_{606}, z_{850}, V_{606}, UV_{336}, I_{814}, J_{125}, Y_{105}, H_{160}, JH_{140}$, and from Spitzer Space Telescope (SST) observations.

For $z = 4$ to 8 we obtain the distributions of galaxy stellar mass M_*/M_{\odot} from Table 2 or Figure 9 of [3] (identified by black square markers in distributions of M_*/M_{\odot}). The analysis in [3] obtains relations between M_*/M_{\odot} and magnitude M_{UV} , for each photometric z , fitting HST images taken with 10 filters, using an SPS model. Then the distributions of M_*/M_{\odot} are obtained with the distributions of magnitude M_{UV} in [25]. As a cross-check we mention that the thick gray lines in Figure 9 of [3], corresponding to Λ CDM predictions, are in agreement with our Λ CDM predictions.

We obtain distributions of galaxy stellar mass M_*/M_{\odot} for $z = 2$ to 8 from Figure 4 of [5], and distributions of star formation rates (SFR) from Figure 1 of [5] (red triangles). These distributions are obtained using the continuity equation for the stellar masses of galaxies, with inputs and comparisons to a large number of sources [5].

For $z = 4$ to 8 we obtain the distributions of galaxy stellar mass M_*/M_{\odot} from Figure 5 of [6] (green triangles). These measurements are based on approximately 3300 galaxy images taken with the James Webb Space Telescope Near Infrared Camera (NIRCam). This data is complemented by the HST Cosmic Assembly Near-Infrared Deep Extragalactic Legacy Survey (CANDELS). The label “ $z = 6$ ” in, e.g. Figure 1, means $z = 6$ for the predictions,

and $5.5 < z < 6.5$ for the measurements. We have neglected the corresponding bias.

Measurements of L_{UV} for $z \geq 8$ from JWST data are obtained from [15], [16], [17], [18], [19], [20], [21], [22], [23] (red triangles). See [26] for an analysis in the Λ CDM scenario. The measurements for $z \gtrsim 11$ need to be considered as “preliminary”, as stated by their authors, for several reasons:

- The measurements at lower z are counting experiments: the galaxy candidates are assigned to bins of magnitude and redshift (M_{UV}, z) and are then counted. At the high- z frontier, the bins (M_{UV}, z) are increased in size so the mean number of counts does not drop below ≈ 1 . The analysis ceases to be a counting experiment, and becomes an extrapolation of a Press-Schechter-like fit to lower z data, keeping all parameters fixed except the normalization. The tension arises at the transition between these two methods.
- To illustrate the low numbers of events, let us mention that the measurements in [15] are based on 33, 22, 16 and 3 galaxy candidates, after correcting for completeness, in the bins $7.5 < z < 8.5$, $8.5 < z < 9.5$, $9.5 < z < 11.5$ and $11.5 < z < 13.5$, respectively. Therefore, where the apparent tension between observations and “first-order” predictions of L_{UV} arise, i.e. $z \gtrsim 11$, there are only about 3 galaxy candidates with photometric redshift. On the other hand, a single galaxy correctly assigned to a bin, i.e. with spectroscopically confirmed redshift z , and a luminosity distribution consistent with stellar expectations (limiting the possible contribution from active galactic nuclei (AGN)), could rule out a theory if the theory predicts one galaxy with a probability less than, say, 0.6%.
- To illustrate the difficulties with the photometric classification of galaxies let us mention that Table 4 of [16] presents an assessment of the “purity” and “completeness” of the selected samples by several authors. A good feeling of the uncertainties is quoted from [16]: “Using all of these samples we then derive UV LF and luminosity density results at $z \geq 8$, finding substantial differences. For example, including the full set of “solid” and “possible” $z \geq 12$ candidates from the literature, we find UV LF and luminosity densities which are $\approx 7\times$ and $\approx 20\times$ higher than relying on the “robust” candidates alone. These results indicate the evolution of the UV LF and luminosity densities at $z \geq 8$ is still extremely uncertain, emphasizing the need for spectroscopy and deeper NIRCcam+optical imaging to obtain reliable results.” Note that

the measurements of L_{UV} in Figures 4 and 5 are based on photometric redshift measurements.

- If AGN contribute to the observed UV luminosity, then the measurements can drop by 0.4 dex on average, or up to 4 dex for individual galaxies [27].
- Corrections for dust attenuation are very uncertain unless data is available in a wide range of wavelengths [5].
- The measurements of L_{UV} presented in Figures 3 to 5 for $z \geq 8$ are not independent as they use overlapping data sets. At $z \geq 11$ there are more measurements than galaxy candidates.
- Cosmic variance becomes important at $z \gtrsim 14$ [28].

The experimental determinations of the galaxy stellar masses M_* depend on stellar population synthesis (SPS) models and spectral energy distributions (SED) models that use images with several filters, and therefore do not include dead star remnants (ejected baryons into inter-stellar space, white dwarfs, neutron stars, and black holes). So measured and predicted M_* do not include dead star remnants.

4 Predictions

This section describes the extension of the Press-Schechter formalism that we use to include warm dark matter (see [14] and [29] for more details). The Press-Schechter prediction [9] is

$$\frac{1}{V} \frac{dn}{d \ln M} = \frac{\bar{\rho}_m}{M} \frac{d \ln(\sigma^{-1})}{d \ln M} f_{\text{PS}}(\nu), \quad (10)$$

where

$$f_{\text{PS}}(\nu) = \sqrt{\frac{2}{\pi}} \nu \exp\left(-\frac{\nu^2}{2}\right), \quad (11)$$

and

$$\nu \equiv \frac{1.686}{\sigma(M, z, k_{fs})}. \quad (12)$$

The factor 1.686 is obtained analytically for spherical collapse with cold dark matter, and becomes valid for warm dark matter when $M \gtrsim M_{vd}$, where M_{vd} is the velocity dispersion cut-off mass. Predictions are presented only for $M > M_{vd}$, see Table 1 of [14]. In the spirit of the present study, we

define our “first-order” prediction, for comparison purposes, with the factor 1.686 unchanged, i.e. independent of M and k_{fs} . The Sheth-Mo-Tormen ellipsoidal collapse extensions [10] [11] are obtained by replacing $f_{\text{PS}}(\nu)$ by $f_{\text{EC}}(\nu)$:

$$f_{\text{EC}}(\nu) = 0.322 [1 + \tilde{\nu}^{-0.6}] f_{\text{PS}}(\tilde{\nu}), \quad (13)$$

with $\tilde{\nu} = \nu$. Good fits to simulations are obtained with $\tilde{\nu} = 0.84\nu$ [11]. The factor 0.84 depends on the algorithm used to identify the collapsed halos.

These predictions depend on the variance of the linear relative density perturbation $\delta(\mathbf{x}) \equiv (\rho(\mathbf{x}) - \bar{\rho})/\bar{\rho}$:

$$\sigma^2(M, z, k_{\text{fs}}) = \frac{f^2}{(2\pi)^3(1+z)^2} \int_0^\infty 4\pi k^2 dk P(k) \tau^2(k) W^2(k). \quad (14)$$

$\sigma^2(M, z, k_{\text{fs}})$ depends on the linear total (dark matter plus baryon) mass scale M at redshift z , and on the comoving cut-off wavenumber k_{fs} due to dark matter free-streaming. $P(k)$ is the comoving power spectrum of linear density perturbations in the cold dark matter Λ CDM cosmology [30]. $W(k)$ is a window function that defines the mass scale M . $\tau^2(k)$ is the power spectrum cut-off factor due to dark matter free-streaming. The factor f is due to the cosmological constant: $f = 0.79, 0.99, 1.00$ for $z = 0, 2, \gg 2$ [30]. Three window functions are considered: the top-hat in r-space, the sharp-k (or top-hat in k-space), and the Gaussian window function:

$$W(k) = \exp\left(-\frac{k^2}{2k_0^2}\right), \quad M = \frac{4}{3}\pi \left(\frac{1.555}{k_0}\right)^3 \bar{\rho}_m. \quad (15)$$

$\bar{\rho}_m$ is the total (dark matter plus baryon) mean density. We use the following form for the free-streaming cut-off factor:

$$\begin{aligned} \tau^2(k) &= \exp\left(-\frac{k^2}{k_{\text{fs}}^2(t_{\text{eq}})}\right) && \text{if } k < k_{\text{fs}}(t_{\text{eq}}), \\ &= \exp\left(-\frac{k^n}{k_{\text{fs}}^n(t_{\text{eq}})}\right) && \text{if } k \geq k_{\text{fs}}(t_{\text{eq}}). \end{aligned} \quad (16)$$

At the time t_{eq} when the matter density begins to dominate, $\tau^2(k)$ has the approximate form (16) with $n = 2$ [31]. Thereafter, $\tau^2(k)$ develops a non-linear regenerated “tail” with n measured to be in the range 0.5 to 1.1 [14]. In the present study we take $n = 1$, and use the Gaussian window function (see studies in [14]). We have verified that the predictions change negligibly for $0.5 < n < 1.1$, and also if the sharp-k window function is used with $n = 1$ [14]. The amplitude of $P(k)$ is adjusted for each k_{fs} so that the relative density root-mean-square fluctuation σ , calculated with the top-hat window function with radius $r = 8/h = 8/0.674$ Mpc, is $\sigma_8 = 0.811$ [7].

5 Discussion

Let us now discuss the discrepancies found in Figures 1 to 5.

1. Discrepancies of L_{UV} distributions at $L_{UV}/L_{\odot} \gtrsim 10^{10.7}$ and $3 \lesssim z \lesssim 9$. This discrepancy is observed in HST and JWST data. This discrepancy is studied in [5], and is (apparently) due to the dust correction of the measured SFR. When the dust correction is based only on the UV slope, the results are inconsistent with other data sets, and the dust-corrected SFR falls short of multi-wavelength determinations at high SFR (dominated by dusty star forming progenitors of present-day quiescent galaxies). A reliable dust correction needs, in addition to the UV images, also optical, radio, $H\alpha$, mid-IR $24 \mu\text{m}$, and far-IR images. The results of the continuity equation [5], based on multi-wavelength dust corrections, are indeed consistent with the predictions as shown in Figures 1 to 3 (see the red triangles in L_{UV} distributions).

2. Discrepancies of M_* distributions at $z \lesssim 5$. This discrepancy can be understood qualitatively, at least in part, as follows (this is my tentative understanding). In the warm dark matter scenario, the first galaxies to form have $M \approx M_{vd} \approx 2 \times 10^8 M_{\odot}$ at $z = 4$, increasing to $\approx 2 \times 10^9 M_{\odot}$ at $z = 10$ (see Table 1 of [14] for $k_{fs} = 2 \text{ Mpc}^{-1}$). Thereafter, the formation of galaxies proceeds hierarchically as larger and larger perturbation masses M become non-linear and collapse due to gravity. Therefore, low mass halos become part of higher and higher mass halos as time goes on, and so become under-counted. In other words, the distribution of low M_* galaxies becomes ill-defined at late times.

3. Discrepancies of preliminary JWST observations of L_{UV} distributions at $z \gtrsim 11$. For $6 \lesssim z \lesssim 10$ the JWST data is in agreement with predictions for $k_{fs} \approx 2 \text{ Mpc}^{-1}$ (see green triangles in Figures 1 to 4). Preliminary JWST observations at $z = 11, 12$ and 13 are in mild tension with the predictions. However these observations need spectroscopic confirmation of the redshifts, and higher statistics, before any conclusions can be presented, see discussion in Section 3 and in [16].

6 Conclusions

We have presented comparisons of measured distributions of galaxy luminosities per unit bandwidth L_{UV} and galaxy stellar masses M_* with “first-order” predictions, as a function of k_{fs} , for z in the range 2 to 13. The only outstanding tension for JWST observations corresponds to L_{UV} with $z \gtrsim 11$. However, these measurements are still preliminary until spectroscopic confirmation of z is obtained, and of limited significance (as stated by the authors,

e.g. [16])

We conclude that the “first-order” predictions with the measured $k_{fs} = 2.0^{+0.8}_{-0.5} \text{ Mpc}^{-1}$ [14], and two parameters $a = 1.5$ and $b = 9.6$, obtained *prior* to JWST data [13] [14], and assumed to be constants independent of (M, z, k_{fs}) , are in agreement with the current data within their theoretical and observational uncertainties. This result is indeed surprising, considering the large range of z and M , with constant star formation efficiency f_* and constant b , and such a basic and simple “first order” prediction model with no new degrees of freedom! The “first-order” predictions are therefore a useful starting point to include more detailed astrophysical models to account for more precise future observations, and to describe other observables, and their evolution.

Can dark matter be cold? Consider, as an example, Figure 1. The distributions of M_*/M_\odot and of L_{UV}/L_\odot are nicely consistent with $k_{fs} \approx 2 \text{ Mpc}^{-1}$ and a constant star formation efficiency $f_* \approx 0.20$. If, however, dark matter is cold, i.e. if k_{fs} is very large, then both M_* and L_{UV} data tells us that f_* at $M \approx 10^9 M_\odot$ is approximately 1/10th of f_* at $M \gtrsim 10^{11} M_\odot$. Is this possible? Supernova and active galactic nuclei (AGN) winds are invoked to explain this low f_* at low M_* . However, three additional and independent indications that dark matter may be warm, with $k_{fs} \approx 2 \text{ Mpc}^{-1}$, are i) the observed distributions of $M = 10^{1.5} M_*$ have a cut-off at approximately M_{vd} (less massive galaxies would have to be “stripped-down” galaxies [29]), ii) the measurements of spiral galaxy rotation curves [32] [33], and iii) the reionization optical depth [14] [34]. Item i) is related to the “missing satellite” problem, and ii) is related to the “core-cusp” problem.

If the preliminary tension of L_{UV} with $z \gtrsim 11$ is confirmed by future observations and analysis, and becomes significant, then we need to let the parameters a and b become functions of z , with $b - a$ growing from 8.1 at $z \lesssim 10$ to approximately 9.1 at $z \gtrsim 11$ (for the case $k_{fs} \approx 2 \text{ Mpc}^{-1}$). In other words, we would have to allow the star formation efficiency f_* to increase above 0.20 at $z \gtrsim 11$, and/or allow first stars to be more massive and luminous than at lower z . Let us work and see.

References

- [1] Gupta, R.P. (2023) JWST early Universe observations and Λ CDM cosmology. Monthly Notices of the Royal Astronomical Society **524** 3, 3385-3395

- [2] Behroozi, P.S., Wechsler, R.H., Conroy, C. (2013) The average star formation histories of galaxies in dark matter halos from $z = 0 - 8$. *The Astrophysical Journal*, 770:57 doi:10.1088/0004-637X/770/1/57
- [3] Song, M., *et al.* (2016) The Evolution of the Galaxy Stellar Mass Function at $z = 4-8$: A Steepening Low-Mass-End Slope with Increasing Redshift. *The Astrophysical Journal*, 825:5
- [4] Bouwens, R.J., *et al.* (2021) New Determinations of the Luminosity Functions from $z \approx 9$ to $z \approx 2$ show Remarkable Consistency with Halo Growth and a Constant Star Formation Efficiency, <https://arxiv.org/pdf/2102.07775.pdf> (HST)
- [5] Lapi, A., Mancuso, C., Bressan, A., Danese, L. (2017), Stellar Mass Function of Active and Quiescent Galaxies via the Continuity Equation. arXiv:1708.07643
- [6] Navarro-Carrera, R., Rinaldi, P., Caputi, K.I., Iani, E., Kokorev, V., van Mierlo, S. (2023) Constraints on the Faint End of the Galaxy Stellar Mass Function at $z \approx 4 - 8$ from Deep JWST Data. arXiv:2305.16141
- [7] Workman, R.L., *et al.* (Particle Data Group) The Review of Particle Physics (2023) *Prog. Theor. Exp. Phys.* 2022, 083C01
- [8] Willmer, C.N.A., (2018) The Absolute Magnitude of the Sun in Several Filters. *The Astrophysical Journal Supplement Series*, 236:47 <https://iopscience.iop.org/article/10.3847/1538-4365/aabfdf/pdf>
- [9] Press, W.H., and Schechter, P. (1974) Formation of galaxies and clusters of galaxies by self-similar gravitational condensation. *The Astrophysical Journal*, **187**, 425-438.
- [10] Sheth R.K., Tormen G., (1999) Large-scale bias and the peak background split. *Mon. Not. R. Astron. Soc.*, **308**, 119-126
- [11] Sheth, R.K., Mo, H.J., Tormen, G. (2001) Ellipsoidal collapse and an improved model for the number and spatial distribution of dark matter haloes. *Mon. Not. R. Astron. Soc.* **323**, 1-12
- [12] Madau, P., Pozzetti, L., Dickinson, M. (1998) The Star Formation History of Field Galaxies, *The American Astronomical Society*. <https://iopscience.iop.org/article/10.1086/305523/pdf>

- [13] Hoeneisen, B. (2020) Fermion or Boson Dark Matter? *International Journal of Astronomy and Astrophysics*, **10**, 203-223. <https://doi.org/10.4236/ijaa.2020.103011>
- [14] Hoeneisen, B. (2022) Measurement of the Dark Matter Velocity Dispersion with Galaxy Stellar Masses, UV Luminosities, and Reionization. *International Journal of Astronomy and Astrophysics*, **12**, 258-272. <https://doi.org/10.4236/ijaa.2022.123015>
- [15] Adams, N. J., Conselice, C. J., Austin, D., et al. (2023), arXiv:2304.13721, doi: 10.48550/arXiv.2304.13721
- [16] Bouwens, R., Illingworth, G., Oesch, P., et al. (2023), MNRAS, 523, 1009, doi: 10.1093/mnras/stad1014
- [17] Donnan, C. T., McLeod, D. J., Dunlop, J. S., et al. (2023), MNRAS, 518, 6011, doi: 10.1093/mnras/stac3472
- [18] Harikane, Y., Ouchi, M., Oguri, M., et al. (2023), ApJS, 265, 5, doi: 10.3847/1538-4365/acaaa9
- [19] Finkelstein, S. L., Bagley, M. B., Ferguson, H. C., et al. (2023), ApJL, 946, L13, doi: 10.3847/2041-8213/acade4
- [20] McLeod, D. J., Donnan, C. T., McLure, R. J., et al. (2023), arXiv:2304.14469, doi: 10.48550/arXiv.2304.14469
- [21] Pérez-González, P. G., Costantin, L., Langeroodi, D., et al. (2023), arXiv:2302.02429, doi: 10.48550/arXiv.2302.02429
- [22] Morishita, T., Stiavelli, M. (2023), ApJL, 946, L35, doi: 10.3847/2041-8213/acbf50
- [23] Naidu, R. P., Oesch, P. A., van Dokkum, P., et al. (2022), ApJL, 940, L14, doi: 10.3847/2041-8213/ac9b22
- [24] Oesch, P.A., Bouwens, R.J., Illingworth, G.D., Labbé, I., Stefanon, M. (2018) The Dearth of $z \approx 10$ Galaxies in All HST Legacy Fields – The Rapid Evolution of the Galaxy Population in the First 500 Myr. *The Astrophysical Journal*, **855**, 105
- [25] Finkelstein, S.L., Papovich, C., Salmon, B., et al. (2012) Candels: The Evolution of Galaxy Rest-frame Ultraviolet Colors from $z = 8$ to 4. *The Astrophysical Journal*, **756**, 164

- [26] Wang, Y., Lei, L., Yuan, G.W., Fan, Y.Z., (2023) Modeling the JWST High-Redshift Galaxies with a General Formation Scenario and the Consistency with the Λ CDM Model. arXiv:2307.12487
- [27] D’Silva, J.C.J., et al (2023) Star formation and AGN activity 500 Myr after the Big Bang: Insights from JWST. arXiv:2310.03081
- [28] Yung, L.Y.A., Somerville, R.S., Finkelstein, S.L., Wilkins, S.M., Gardner, J.P., (2023) Are the ultra-high-redshift galaxies at $z > 10$ surprising in the context of standard galaxy formation models? arXiv:2304.04348
- [29] Hoeneisen, B. (2022) Comments on Warm Dark Matter Measurements and Limits. *International Journal of Astronomy and Astrophysics*, **12**, 94-109. <https://doi.org/10.4236/ijaa.2022.121006>
- [30] Weinberg, S. (2008) *Cosmology*, Oxford University Press, Oxford OX2 6DP.
- [31] Boyanovsky, D., de Vega, H.J., Sanchez, N.G. (2008) The dark matter transfer function: free streaming, particle statistics and memory of gravitational clustering. arXiv:0807.0622
- [32] Hoeneisen, B. (2023) Understanding the Formation of Galaxies with Warm Dark Matter. *Journal of Modern Physics*, **14**, 1741-1754. <https://doi.org/10.4236/jmp.2023.1413103>
- [33] Hoeneisen, B. (2022) Measurement of the Dark Matter Velocity Dispersion with Dwarf Galaxy Rotation Curves. *International Journal of Astronomy and Astrophysics*, **12**, 363-381. <https://doi.org/10.4236/ijaa.2022.124021>
- [34] Lin, H., Gong, Y., Yue, B., Chen, X. (2023) Implication of the Stellar Mass Density of High- z Massive Galaxies from JWST on Warm Dark Matter. arXiv:2306.05648